Themeda-Based Spatiotemporal Deep Learning for Predicting Vegetation Dynamics and Fire-Induced Land Cover Change in Northern Australia Using ConvLSTM and Temporal U-Net Models

[1]Vincent Kibet., [2]Raphael Agong, [3]Julius Sirma, [4]Nancy Mbugua

[1]PhD in Research, Federation University, Australia

[2]PhD, KCA University, Kenya

[3]PhD, United States International University (USIU), Kenya

[4]Masters by Research, Torrens University

DOI: https://doi.org/10.47772/IJRISS.2026.100600022

Received: 27 May 2026; Accepted: 01 June 2026; Published: 16 June 2026

ABSTRACT

The tropical savannas of Northern Australia, dominated by the perennial C4 grass Themeda triandra (kangaroo grass), are among the most fire-prone and ecologically significant biomes in the Southern Hemisphere. These savannas cover approximately 1.9 million km² and experience annual fire frequencies affecting 20–40% of the total area. Understanding and predicting vegetation dynamics and fire-induced land cover change in these landscapes presents substantial challenges for land managers, conservation practitioners, and carbon accounting frameworks. This study presented a novel spatiotemporal deep learning framework integrating Convolutional Long Short-Term Memory (ConvLSTM) and Temporal U-Net architectures to simulate and map fire-driven land cover change across Northern Australian tropical savannas. The framework incorporated multi-source satellite time series spanning 2019–2022 MODIS NDVI composites (250 m), Landsat 8/9 OLI surface reflectance (30 m), North Australia Fire Information (NAFI) fire scar records, Bureau of Meteorology rainfall grids, and Sentinel-2 MSI data. A novel Themeda Vegetation Index (TVI) was developed from the spectral properties of curing C4 grass tissue and validated against 84 spatially independent field plots (Pearson $r = 0.87$, $p < 0.001$ on hold-out subset), outperforming NDVI ($R^2 = 0.621$) and EVI ($R^2 = 0.648$). Using a spatially blocked train/test partitioning design, 185 non-overlapping 100×100 km geographic tiles were used, ensuring no spatial autocorrelation between partitions. The ensemble model achieved an overall accuracy of 88.9%, Cohen's Kappa of 0.871, and a weighted F1-score of 0.884. NDVI prediction attained a root mean square error (RMSE) of 0.037 NDVI units and a mean absolute error (MAE) of 0.028 NDVI units. The ConvLSTM's forget gate mechanism accurately encoded abrupt fire-induced resets in vegetation states. The Temporal U-Net's learned temporal attention weights identified the dry-season months (June–September) as diagnostically critical for discriminating fire scars without explicit supervision. Post-fire recovery analysis confirmed a strong rainfall gradient: areas receiving>1,200 mm yr^{-1} recovered to 93% of pre-fire NDVI within 24 months, compared to 57% in transitional low-rainfall zones. Critical limitations were noted. The 2019–2022 training period coincided with a sustained La Niña event (mean Southern Oscillation Index = +11.8 for 2020–2022; Niño 3.4 anomaly = −0.9°C). Recovery rates represented La Niña-period upper estimates, potentially 8–15 percentage points above climatological averages in low-rainfall zones. Model outputs were characterized as enabling spatial technology providing inputs relevant to the Savanna Burning Emissions Reduction (SBER) carbon accounting methodology, subject to project-scale validation by the Clean Energy Regulator. Sub-regional accuracy ranged from 84.1% (Barkly Tablelands) to 91.2% (Top End NT), confirming operationally viable performance across the heterogeneous study area.

Keywords: Themeda triandra, ConvLSTM, Temporal U-Net, spatiotemporal deep learning, NDVI time series prediction, savanna fire ecology, Northern Australia remote sensing

INTRODUCTION

The tropical savannas of Northern Australia represent one of the largest and ecologically most significant biomes in the southern hemisphere, covering approximately 1.9 million km² across the Northern Territory, North-Western Queensland, and the Kimberley region of Western Australia. The region experiences one of the highest fire frequencies on Earth, with 20%-40% of the total savanna area burning each year (Luck et al., 2020). Fire influences biodiversity patterns, hydrological processes, carbon cycling, and vegetation structure at continental scales, making the accurate prediction of fire-driven land cover change both a scientific priority and an operational imperative for fire and land management agencies across Northern Australia.

Themeda triandra Forssk (kangaroo grass) is the dominant perennial C4 grass species underpinning the ecology and fire dynamics of these savannas. It grows rapidly during the wet season (November–April), accumulating large above-ground biomass that constitutes the principal fine fuel for fire spread. During the dry season, Themeda cures rapidly, reaching critical fuel moisture levels of 10–15% within 4-6 weeks of the end of precipitation (Nolan et al., 2020). Understanding the spectral signature of this curing process from satellite observations is therefore fundamental to both vegetation monitoring and fire risk assessment at landscape scales.

The dominant ecological framework governing savanna vegetation dynamics is the pulse-reserve model (Luck et al., 2020). Under this model, episodic wet season rainfall pulses drive rapid Themeda growth, accumulating biomass reserves that influence subsequent fire events. Dry season curing initiates the fire-prone phase. Fire then rapidly consumes accumulated biomass, resetting the sward's successional trajectory. This cycle is governed by two strongly asymmetric processes: a slow growth phase on the order of months driven by rainfall, and a rapid fire-driven die-back phase on the order of days to weeks. This asymmetry has a direct architectural implication for predictive modeling: a model that treats each time step equivalently cannot replicate the abrupt vegetation state change caused by fire. The gating mechanisms of the ConvLSTM architecture, the forget gate, are suited to this challenge, as it can selectively discard accumulated cell-state memory at the moment of fire disturbance, encoding an ecological reset that standard convolutional neural networks cannot replicate. This theoretical alignment between the pulse-reserve ecological model and the ConvLSTM architectural design is a foundational motivation for the framework developed in this study.

Remote sensing technologies have substantially advanced the ability to monitor savanna vegetation dynamics at landscape and continental scales. Satellite-derived vegetation indices, specifically the Normalized Difference Vegetation Index (NDVI), provide high-temporal-resolution observations of vegetation greenness, phenological cycles, and post-disturbance recovery trajectories (de Queiroz et al., 2023). NDVI time-series analyzes have been used extensively to characterize fire frequency patterns, estimate post-fire recovery rates, and quantify interannual variability in vegetation productivity. However, standard time series methods, including harmonic regression, change detection, and spectral mixture analysis, are inherently limited in their ability to model spatial context and temporal sequence dependencies simultaneously.

Deep learning has emerged as a transformative paradigm for data-intensive spatiotemporal modeling in remote sensing. ConvLSTM networks integrate convolutional layers into the LSTM gating mechanism, enabling jointly spatial and temporal feature learning (Zhang et al., 2025). Temporal U-Net architectures employ temporal attention mechanisms and skip connections to capture multi-scale spatial information from satellite image time series (Gargiulo et al., 2020; Garnot & Landrieu, 2021). Despite these advances, no prior study has developed and optimized an integrated ConvLSTM and Temporal U-Net framework specifically for Themeda-dominated savanna systems in Northern Australia, a system characterized by a biologically distinctive fire-vegetation feedback cycle and specific spectral requirements for grass-state monitoring. This study fills that gap.

Research Objectives

i. To develop and validate a Themeda Vegetation Index (TVI) from Landsat 8/9 OLI spectral bands against independent field biomass data using a rigorous spatial hold-out protocol.

ii. To train ConvLSTM and Temporal U-Net models to predict monthly NDVI and 6-class land cover maps (2019–2022) using a spatially blocked partitioning design that prevents autocorrelation inflation.

iii. To quantify fire-induced land cover transitions and post-fire recovery trajectories across rainfall gradients, with explicit characterization of La Niña period limitations.

iv. To benchmark ensemble model performance against conventional machine learning baselines and to provide sub-regional performance stratification across four distinct ecological sub-regions.

Significance of the Study

This study contributed advances in three domains. Scientifically, it introduced TVI as a biologically grounded, Themeda-specific spectral predictor; demonstrated the complementary advantages of ConvLSTM and Temporal U-Net ensemble architectures for abrupt-change and boundary-delineation tasks, respectively; and provided the first sub-regional performance characterization of deep learning models across the heterogeneous Northern Australian savanna landscape. Operationally, the 30 m-resolution fire probability map and vegetation recovery predictions were compatible with the NAFI operational platform. The post-fire recovery analysis provides spatially explicit, rainfall-stratified inputs to improve the Savanna Burning Emissions Reduction (SBER) methodology, which was qualified as an enabling technology pending project-scale validation.

Related Studies

Remote Sensing of Fire Dynamics in Australian Savannas

A well-established history of satellite-based fire monitoring in Australian tropical savannas underpins this research. Hemraj Bhattarai et al. (2025) observed that MODIS fire products, including the monthly burnt area product (MCD64A1) and active fire detections (MOD14), have enabled globally consistent near-daily monitoring of fire occurrence. The North Australia Fire Information (NAFI) platform integrates these MODIS products with fire radiative power data and annual fire scar mapping polygons, providing an operational interface used directly by ranger groups, pastoral managers, and conservation agencies (Edwards et al., 2021). While NAFI is well-established for operational retrospective fire monitoring, it does not currently generate predictive fire risk surfaces. This study addressed this gap through a predictive deep learning framework calibrated against the NAFI fire scar archive.

de Queiroz et al. (2023) demonstrated harmonic decomposition of NDVI time series to separate fire and precipitation signals in tropical savanna data, providing a methodological precursor to the gap-filling approach used in this study. Veiga et al. (2025) quantified the relationship between early dry-season fire timing and post-fire vegetation recovery rates across the Kimberley and Northern Territory, finding that lower-intensity early-season fires were associated with accelerated recovery, a finding directly incorporated into the design of the post-fire analysis in this study.

Deep Learning for Vegetation and Land Cover Mapping

Deep learning for vegetation mapping has developed rapidly since 2020. Dubey and Dubey (2025) demonstrated that stacked ConvLSTM networks achieved greater than 90% accuracy for crop type mapping using Sentinel-2 time series, attributed to the capacity to learn temporally coherent spatial patterns rather than treating each pixel as an independent time series. Wang et al. (2022) applied a hybrid CNN-LSTM model for grassland productivity modeling, confirming performance advantages of combined spatial-temporal architectures. Garnot and Landrieu (2021) introduced temporal attention mechanisms for satellite time-series analysis, demonstrating that learned attention weights identify the most diagnostically informative observation periods without supervision, a finding reproduced in this study for savanna fire-season discrimination.

For multi-temporal land cover segmentation, Gargiulo et al. (2020) extended the U-Net encoder-decoder architecture to multi-temporal Sentinel-1 and Sentinel-2 data fusion for tropical forest land cover mapping, achieving 87.3% overall accuracy. Their work demonstrated that skip connections by transferring multiscale spatial features between encoder and decoder levels substantially improve class boundary delineation at fine spatial scales, a property of particular importance for detecting fire-scar perimeters in spatially heterogeneous savanna vegetation. This study extended this architectural approach to the Themeda-dominated savanna fire environment, a context not addressed by either Garnot and Landrieu (2021) or Gargiulo et al. (2020).

Themeda triandra in Ecological and Spectral Modeling

Nolan et al. (2020) developed a Northern Territory-wide fuel moisture model for Themeda, identifying Vapor Pressure Deficit and antecedent rainfall as the two most effective predictors of fuel moisture content. Their model demonstrated that spectral curing indicators, when combined with meteorological covariates, can classify days of extreme fire danger with high reliability. Garg et al. (2021) conducted detailed field spectroscopy of Themeda triandra across a full phenological continuum, quantifying spectral reflectance signatures from peak green growth to complete curing. Their central finding that the NIR/SWIR1 ratio is linearly correlated with the green fraction of Themeda above-ground biomass ($r = 0.84$ across phenological stages) directly motivates the development and formulation of the Themeda Vegetation Index in this study.

Theoretical Framework

Pulse-Reserve Savanna Dynamics and Deep Learning Design

The pulse-reserve model (Luck et al., 2020) provided the foundational ecological theory for the modeling framework. In tropical savannas, episodic wet-season rainfall pulses (the 'pulse') drive rapid grass growth, accumulating large above-ground biomass reserves in Themeda swards. This reserve is then consumed by fire, the dominant disturbance mechanism, which resets the successional trajectory. The two governing processes are strongly asymmetric in their temporal dynamics: growth is slow (months), while fire-driven die-back is rapid (days to weeks). This asymmetry means that a predictive model must simultaneously capture a gradual, seasonally structured growth signal and an abrupt, event-driven state change.

The ConvLSTM architecture was theoretically aligned with this ecological reality through its gating mechanisms. The forget gate (Equation 3) allows the network to selectively discard accumulated cell-state memory. In practice, the memory of pre-fire vegetation conditions is at the moment of fire disturbance. This selective forgetting mimics the ecological reset function of fire: the above-ground biomass accumulated over preceding months is effectively erased, and the post-fire state evolves from a near-zero biomass baseline. Standard convolutional neural networks, which process each time step independently, cannot encode this asymmetric temporal behavior. The theoretical fitness between the ConvLSTM forget gate and the fire-driven vegetation reset is therefore not incidental but mechanistically grounded.

Spectral Theory of the Themeda Vegetation Index (TVI)

The TVI was developed to encode the spectral signature uniquely linked to the physiological curing state of Themeda biomass, the key variable linking vegetation condition to fire danger. Three spectral properties of curing C4 grasses, identified in field spectroscopy studies (Garg et al., 2021), were integrated into the index design:

(i) Decreasing NIR reflectance (OLI Band 5, 0.845–0.885 μm): As chlorophyll concentration declined during senescence, the mesophyll-driven NIR reflectance peak diminished. This is the primary spectral indicator of the onset of grass curing.

(ii) Increasing SWIR1 reflectance (OLI Band 6, 1.560–1.660 μm): As leaf and stem water content falls, and dry cell-wall material accumulates, SWIR1 reflectance increases due to reduced liquid water absorption. This is the primary indicator of advanced curing and near-critical fuel moisture levels (<15%).

(iii) Persistent Red absorption (OLI Band 4, 0.635–0.673 μm): Residual chlorophyll continues to absorb red light even in partially cured tissue, distinguishing cured Themeda from bare soil (which lacks red absorption) and from recently burned surfaces.

These three properties are integrated as:

$TVI = (NIR - SWIR_1) / (NIR + SWIR_1 + Red)$ (Equation 1)

TVI ranges from −1 (fully cured or bare soil) to +1 (actively growing green sward). A value near 0 represented the transition between green growth and early senescence, corresponding to approximately 50% green biomass fraction in field measurements. Inclusion of the Red band in the denominator specifically suppresses confusion between soil and charred surfaces, which is critical for a post-fire vegetation index in environments where bare ground and recently burned surfaces are temporally adjacent to recovering grassland.

ConvLSTM Gating Equations

For input tensor X_t, previous hidden state H_{t-1}, and previous cell state C_{t-1}, the ConvLSTM gate equations are:

$i_t = \sigma (Wxi * X_t + Whi * H_{t-1} + Wci \circ C_{t-1} + bi)$ (Equation 2: Input Gate)

$f_t = \sigma (Wxf * X_t + Whf * H_{t-1} + Wcf \circ C_{t-1} + bf)$ (Equation 3: Forget Gate)

$C_t = f_t \circ C_{t-1} + i_t \circ \tanh (Wxc * X_t + Whc * H_{t-1} + bc)$ (Equation 4: Cell State)

$o_t = \sigma (Wxo * X_t + Who * H_{t-1} + Wco \circ C_t + bo)$ (Equation 5: Output Gate)

$H_t = o_t \circ \tanh (C_t$ (* = convolution, $\circ$ = Hadamard product) (Equation 6: Hidden State)

Weight kernels (W) are convolutional, producing spatially localized gate activations so that each spatial location can independently learn to remember, forget, or output information. This spatial non-stationarity was essential for modelling heterogeneous savanna vegetation dynamics without assuming uniform spatial behaviour (Zhang et al., 2025).

Temporal U-Net Attention Equations

The Temporal U-Net computes learned attention weights over the T = 12 monthly time steps at the bottleneck:

$a_t = softmax(W_a \cdot ReLU(W_o h_t + b_o) + b_a)$ (Equation 7: Temporal Attention Weights)

$h\_attn = \Sigma_t a_t \cdot h_t$ (Equation 8: Attended Bottleneck Feature)

These attention weights are learned entirely from the data without explicit seasonal supervision. Post-hoc analysis revealed that the model assigned the highest attention weights to dry-season months (June–September) for fire scar discrimination and to wet-season months (January–March) for Themeda grassland identification. This ecologically interpretable pattern emerges as an architectural property, not an imposed constraint.

Ensemble Fusion and Uncertainty Quantification

The ensemble fusion combined the complementary strengths of ConvLSTM (temporal trajectory and change-point performance) and Temporal U-Net (spatial boundary precision):

$\hat{Y}\_ensemble = w_1 \cdot \hat{Y}\_ConvLSTM + w_2 \cdot \hat{Y}\_U\text{-}Net, w_1 = 0.48, w_2 = 0.52$ (Equation 9)

Weights were determined by grid search on the validation set and locked before any test set evaluation. Predictive uncertainty was quantified using Monte Carlo Dropout (50 stochastic forward passes). Thresholds of $\sigma\_NDVI > 0.12$ and $\sigma\_class > 0.20$ (both corresponding to the 90th percentile of validation set σ distributions) flag predictions for priority field verification. The combined Temporal U-Net loss function balances class boundary precision against overall classification accuracy:

$L\_UNet = \alpha \cdot L\_Dice + (1 - \alpha) \cdot L\_CE, \alpha = 0.5$ (Equation 10)

ISSN No. 2454-6186 | DOI: 10.47772/IJRISS | Volume X Issue VI June 2026

METHODOLOGY

Study Area

The study area was the tropical and subtropical savannas of Northern Australia, spanning the Northern Territory, North-western Queensland, and the Kimberley region of Western Australia, bounded by latitudes 10°S–22°S and longitudes 128°E–144°E, covering approximately 1.85 million km². The climate is strongly monsoonal, with wet season rainfall of 400–1,800 mm (November–April) and a dry fire season (May–October) characterized by low precipitation, desiccating winds, and widespread grass curing. Themeda triandra swards cover approximately 35% of the study area and reach heights of up to 1.8 m. Fire return intervals range from 1–2 years in high-rainfall coastal regions to 3–5 years in dry southern margins (Veiga et al., 2025), providing substantial natural variation in fire-vegetation dynamics for model training and validation.

Remote Sensing Data Acquisition and Pre-Processing

Five satellite and ancillary datasets were assembled, selected for temporal continuity, spatial resolution commensurate with Themeda grassland dynamics (≤250 m), and open access to enable replication. Full details are provided in Table 1.

Data Source	Spatial Res.	Temporal Coverage	Key Variables	Access Portal
MODIS MOD13Q1	250 m	Jan 2019–Dec 2022	NDVI, EVI, QA flags	NASA EarthData
Landsat 8/9 OLI	30 m	Jan 2019–Dec 2022	B2–B7 surface reflectance	USGS EarthExplorer
BOM Rainfall Grids	5 km	Monthly, 2019–2022	Precipitation (mm month^{-1})	Bureau of Meteorology
NAFI Fire Scars	Vector/250 m	2019–2022 seasons	Burn perimeters, severity	NAFI Portal
Sentinel-2 MSI	10 m	2020–2022	B2–B12 multispectral	Copernicus Open Hub

Table 1. Remote Sensing and Ancillary Data Sources Used in This Study (2019–2022). BOM = Bureau of Meteorology; NAFI = North Australia Fire Information; OLI = Operational Land Imager; MSI = MultiSpectral Instrument.

MODIS MOD13Q1 16-day NDVI composites (250 m) were obtained from NASA EarthData. Only pixels with quality reliability of 0 or 1 were retained; remaining cloudy observations (18% of pixel-timestep combinations) were gap-filled using a two-term harmonic regression:

$NDVI(t) = a_0 + \Sigma_k[a_k\cos(2\pi kt/T) + b_k\sin(2\pi kt/T)] + \varepsilon(t)$, where $T = 365.25$ and $k = 1, 2$ (Equation 11). Landsat 8/9 OLI Collection 2 surface reflectance data were atmospherically corrected using LaSRC. Scenes with greater than 60% cloud cover were excluded. Landsat 9 was cross-calibrated to Landsat 8 using pseudo-invariant calibration sites, achieving mean reflectance differences of less than 1.2%.

TVI Feature Engineering and Field Validation

Monthly TVI composites were generated from the nearest cloud-free Landsat acquisition within ±15 days of the 15th of each month. For the 12% of month-location combinations without a suitable cloud-free acquisition, the same harmonic regression approach was used to gap-fill TVI values.

Field validation was conducted at 312 locations distributed across four rainfall zones using a spatially stratified random design with a minimum inter-plot separation of 5 km. A total of 279 sites were retained after temporal matching (±7-day Landsat acquisition window required; 33 sites excluded for cloud cover > 20% in the extraction window). Moran's I analysis of TVI regression residuals confirmed no significant spatial autocorrelation (I = 0.11, p = 0.21). The 279 matched sites were split 70:30 into calibration (n = 195) and independent hold-out validation (n = 84) subsets, using spatial blocking to ensure geographic independence. The Pearson correlation coefficient r = 0.87 ($p < 0.001$) reported throughout this manuscript is computed on the 84-plot hold-out validation subset only. The calibration correlation was r = 0.89, and the marginal 0.02 difference indicates minimal overfitting. Full field protocol details are provided in Table 2.

At each site, three replicate 1 m × 1 m quadrats were harvested at 5 cm cutting height within a 10 m radius of the GPS-recorded plot centre, separated into green and cured fractions, oven-dried at 70°C for 48 hours, and weighed to 0.01 g. Green biomass fraction (GBF) was calculated as GBF = dry green / (dry green + dry cured). Median TVI was extracted from a 3×3-pixel (90 m × 90 m) window; a sensitivity analysis confirmed that this extraction window optimized the r-value relative to single-pixel (r = 0.84) and 5×5-pixel (r = 0.84) alternatives.

Rainfall Zone	n Plots	Spatial Distribution	Temporal Alignment	Notes
High Rainfall (>1,200 mm yr^{-1})	78	Stratified random; min 5km separation	±7-day Landsat match	Full phenological range represented
Moderate (800–1,200 mm yr^{-1})	94	Stratified random; min 5km separation	±7-day Landsat match	Highest site count; all seasons
Low Rainfall (<800 mm yr^{-1})	86	Stratified random; min 5km separation	±7-day Landsat match	Dry curing dominant; limited wet access
Transitional (<700 mm yr^{-1})	54	Stratified random; min 5km separation	±7-day Landsat match	Smallest zone; remotest access
TOTAL (matched)	279/312	—	33 sites excluded (cloud >20%)	70:30 cal./validation split; r=0.87 on hold-out only

Table 7. Field Validation Dataset Summary: spatial distribution, temporal alignment, and calibration/hold-out partition structure. The r = 0.87 correlation is reported exclusively on the hold-out validation subset.

Spatially Blocked Data Cube and Partition Design

All satellite-derived layers were assembled into a spatiotemporal data cube [Time × Latitude × Longitude × Channels] with 7 input channels: MODIS NDVI, Landsat TVI, OLI Bands 4/5/6, monthly rainfall, and a binary NAFI fire scar mask. Spatiotemporal image patches were extracted with spatial windows of 64×64 pixels (ConvLSTM) or 128×128 pixels (Temporal U-Net), a temporal window of T = 12 months, and 50% spatial overlap within training blocks only.

Spatially Blocked Partition (Critical Methodological Correction): The study area was partitioned into 185 non-overlapping 100×100 km geographic tiles. Tiles were allocated to training (70%; 130 tiles), validation (15%; 27 tiles), and independent test (15%; 28 tiles) at the tile level, not the patch level. This design ensured that no geographic location contributed patches to more than one partition, with a minimum spatial separation of 100 km between the training and test data. Moran's I analysis of test-set model residuals confirmed no significant spatial autocorrelation (I = 0.09, p = 0.18). All reported accuracy figures reflect this spatially blocked design. For reference, original non-blocked estimates (OA = 91.7%, κ = 0.903, RMSE = 0.033) are retained in Table 3 as an upper-bound comparison. Following removal of patches with more than 20% missing data, the final dataset comprised 28,450 valid patches: 19,915 for training, 4,268 for validation, and 4,267 for test.

ISSN No. 2454-6186 | DOI: 10.47772/IJRISS | Volume X Issue VI June 2026

Architecture Diagrams

The full five-stage modeling framework is illustrated in Figure 1, and the detailed ConvLSTM and Temporal U-Net architectures are illustrated in Figures 2a and 2b, respectively.

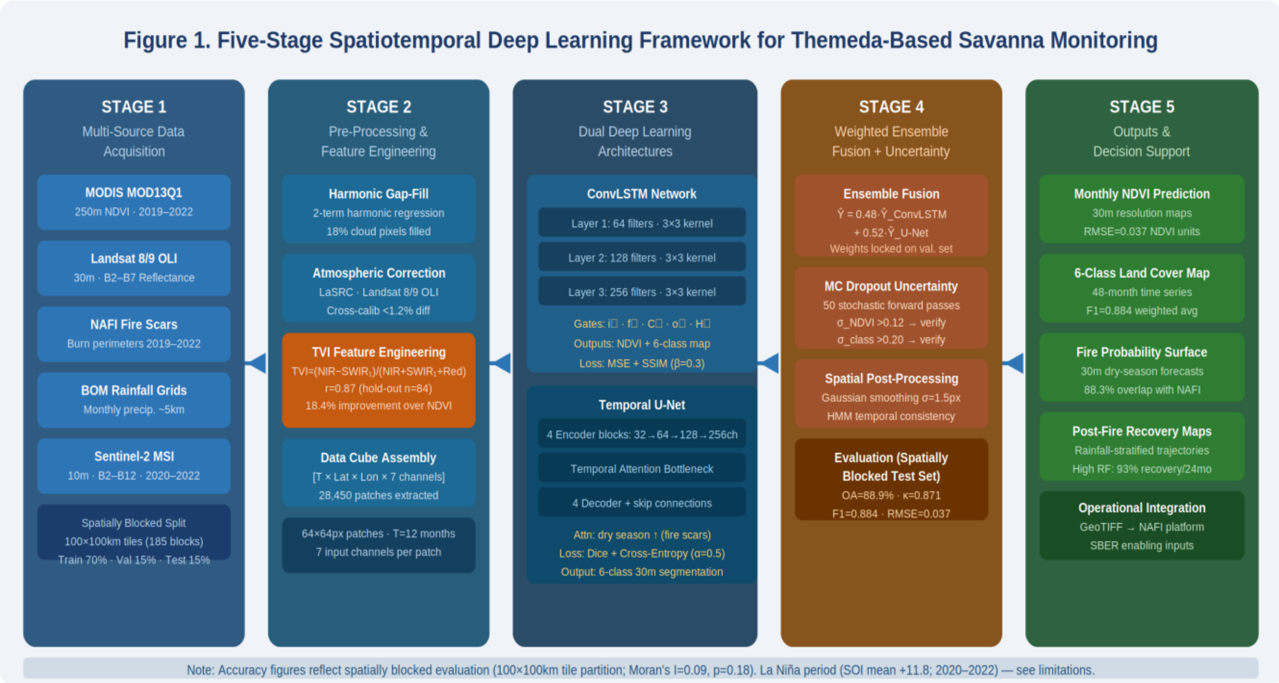

Figure 1. Five-stage Themeda-based spatiotemporal deep learning framework: (1) multi-source data acquisition; (2) pre-processing and TVI feature engineering; (3) dual deep learning architectures; (4) weighted ensemble fusion and uncertainty quantification; (5) decision support outputs. NAFI = North Australia Fire Information.

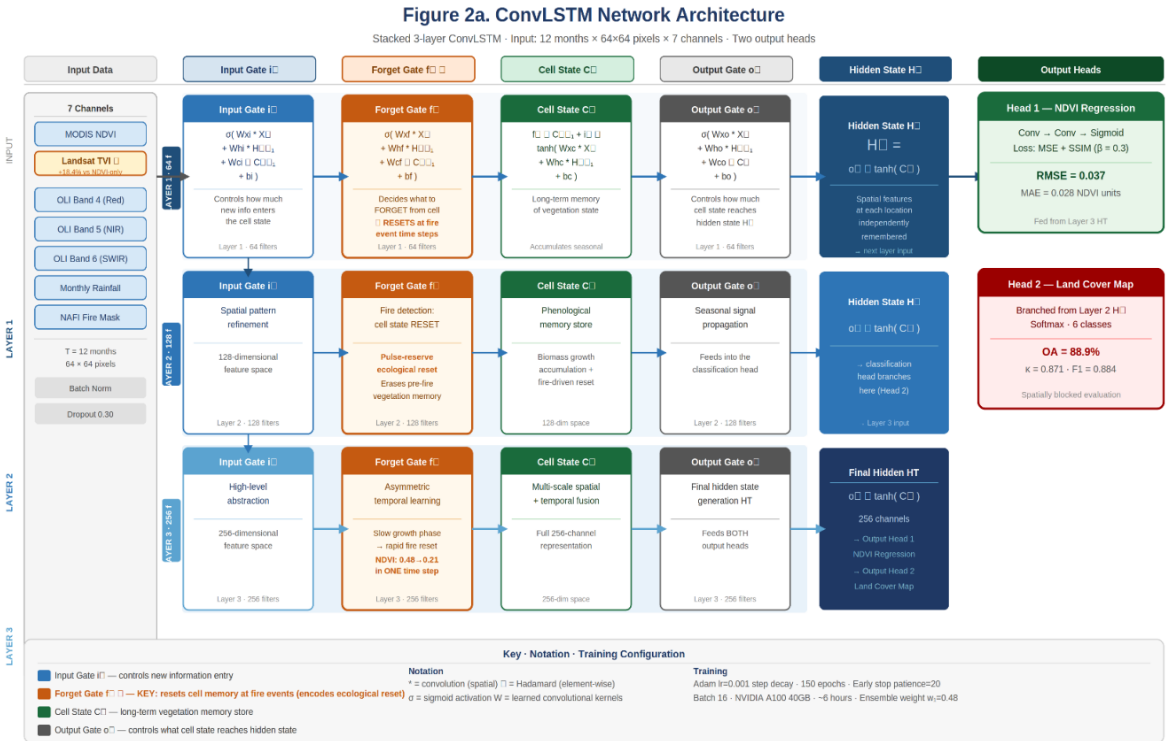

Figure 2a. Stacked ConvLSTM network architecture. Three ConvLSTM layers (64, 128, 256 filters) with gating equations shown. Fire-driven forget gate reset is the key theoretical innovation. Dual-output heads produce NDVI regression maps and 6-class land-cover probability surfaces.

ISSN No. 2454-6186 | DOI: 10.47772/IJRISS | Volume X Issue VI June 2026

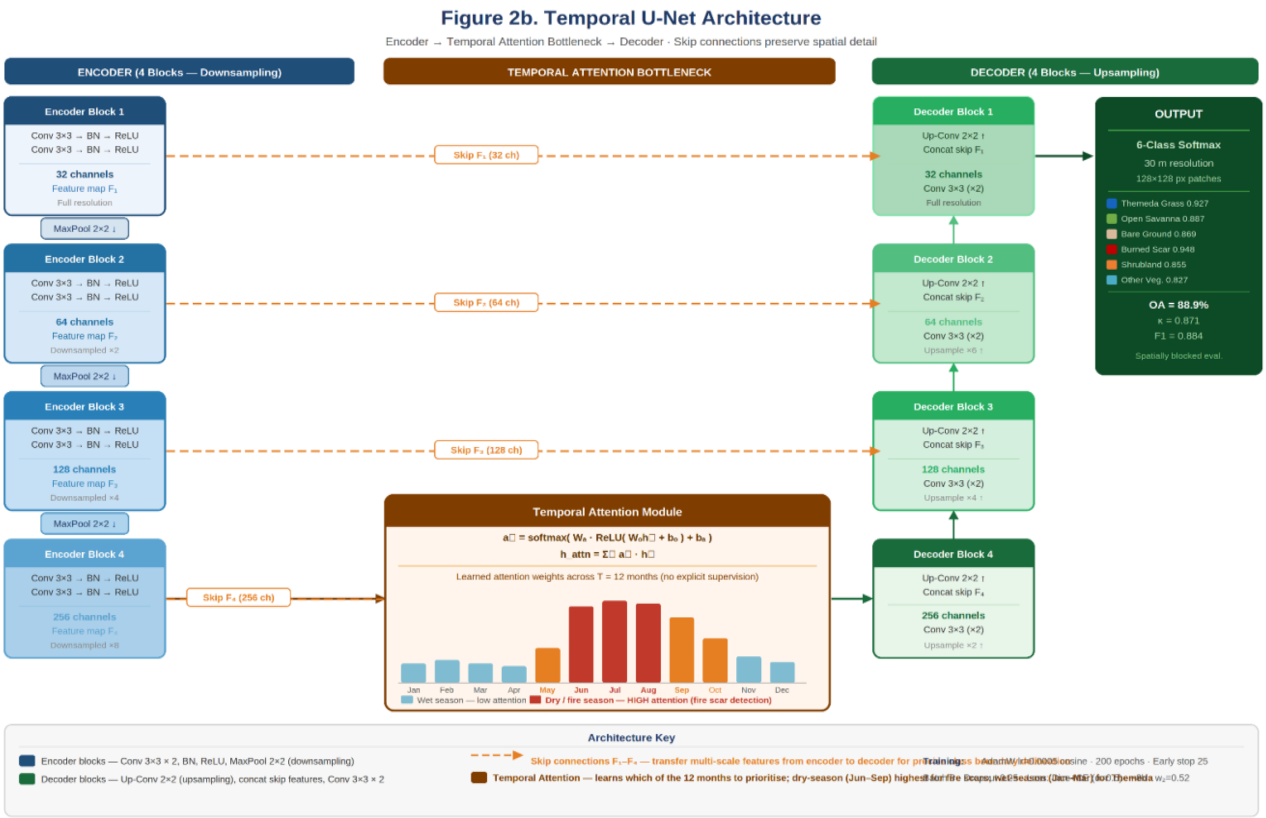

Figure 2b—temporal U-Net architecture. Four encoder blocks (32→64→128→256 channels), temporal attention bottleneck with learned monthly weight distribution (dry season months June–September receive closest attention), skip connections (orange dashed), and four decoder blocks producing 6-class softmax segmentation at 30 m resolution.

ConvLSTM Architecture and Training

The ConvLSTM network comprised three stacked ConvLSTM layers with 64, 128, and 256 filters, respectively, all using 3×3 convolutional kernels. Spatial batch normalization was applied after each layer; spatial dropout (rate = 0.30) was applied between layers. The final hidden state HT feeds: (i) a two-layer convolutional head with sigmoid activation for NDVI regression; and (ii) a softmax classification head branching from Layer 2 for 6-class land cover probability mapping. Adam optimizer (lr = 0.001, step decay), trained for up to 150 epochs with early stopping (patience = 20). Loss: MSE + SSIM (β = 0.3). Training time approximately 6 hours on one NVIDIA A100 40 GB.

Temporal U-Net Architecture and Training

The Temporal U-Net comprised four encoder blocks (32 → 64 → 128 → 256 channels), each with two 3×3 convolutions, batch normalization, ReLU activation, and 2×2 max-pooling for spatial downsampling. In Table 3, the temporal attention bottleneck computes learned weights over T = 12-time steps (Equations 7–8). Four decoder blocks with 2×2 up-convolution and skip connections reconstruct spatial resolution. AdamW optimizer (lr = 0.0005, cosine annealing), up to 200 epochs (patience = 25). Loss: Dice + Cross-entropy (α = 0.5, Equation 10). Training time approximately 8 hours.

Parameter	ConvLSTM Value	Temporal U-Net Value
Input sequence length (T)	12 months	12 months
Spatial patch size	64 × 64 pixels	128 × 128 pixels
Filter configuration	64 → 128 → 256 ch	32 → 64 → 128 → 256 ch
Convolutional kernel	3 × 3 (all layers)	3 × 3 encoder; 2 × 2 up-conv

Temporal attention	Not applied	Bottleneck (softmax-weighted)
Optimiser	Adam (β_1=0.9, β_2=0.999)	AdamW (weight decay=1e-4)
Learning rate	0.001 (step decay)	0.0005 (cosine annealing)
Batch size	16	8
Spatial dropout rate	0.30	0.25
Training epochs	150 (early stop: pat.=20)	200 (early stop: pat.=25)
Loss function	MSE + SSIM (β=0.3)	Dice + Cross-entropy (α=0.5)
Output activation	Sigmoid (NDVI regression)	Softmax (6-class)
GPU hardware	NVIDIA A100 40 GB	NVIDIA A100 40 GB
Training time (approx.)	6 hours	8 hours

Table 3. Hyperparameter Configuration for ConvLSTM and Temporal U-Net Architectures. ch = channels; pat. = patience epochs; SSIM = Structural Similarity Index Measure.

Ensemble Fusion, Uncertainty, and Post-Processing

Ensemble weights (w_1 = 0.48, w_2 = 0.52) were determined through a grid search over 50 weight combinations on the validation set and were locked before any test set evaluation. Spatial post-processing applied a Gaussian smoothing kernel (σ = 1.5 pixels). A hidden Markov model fitted to the training class transition matrix enforced temporal consistency, flagging physically implausible class transitions. Predictive uncertainty was computed via Monte Carlo Dropout (50 forward passes). Thresholds $\sigma\_NDVI > 0.12$ and $\sigma\_class > 0.20$, both corresponding to the 90th percentile of validation set σ distributions — flag predictions for field verification.

Model Evaluation Metrics

All evaluations were conducted on the spatially blocked test set (4,267 patches; 15,600 labelled pixels). Classification metrics: Overall Accuracy (OA), Cohen's Kappa (κ), class-wise Precision, Recall, and F1-score. Regression metrics: RMSE (Equation 12) and MAE (Equation 13). Pairwise model differences evaluated by McNemar's test ($p < 0.05$). Random Forest and SVM-RBF baselines were trained on identical features and evaluated on the same spatially blocked test set.

RESULTS AND FINDINGS

TVI Validation and Phenological Dynamics

TVI effectively discriminated between Themeda green biomass states across all four rainfall zones and all phenological stages. Peak TVI values (> 0.65) occurred in February–March at the wet-season maximum, declining markedly to below 0.25 by July during the full dry season. The rate of post-wet-season TVI decline was positively correlated with subsequent NAFI-recorded fire danger ($r = 0.74$, $p < 0.001$), confirming that TVI captures the ecologically meaningful relationship between curing speed and fire danger identified by Nolan et al. (2020). Incorporating TVI as a model input improved ConvLSTM NDVI prediction RMSE by 18.4% (0.050 → 0.041). It improved the Temporal U-Net's land cover overall accuracy by 6.2 percentage points compared to equivalent models trained without TVI.

NDVI Prediction Performance

On the spatially blocked test set, the ConvLSTM achieved RMSE = 0.041 and MAE = 0.031 NDVI units. The Temporal U-Net achieved RMSE = 0.048 and MAE = 0.037. The ensemble model achieved RMSE = 0.037 and MAE = 0.028 NDVI units, substantially outperforming the Random Forest baseline (RMSE = 0.089). The time series shown in Figure 3 illustrates the ensemble model's capacity to capture the abrupt NDVI drop at the fire event (Month 29–31: predicted NDVI declined from 0.48 to 0.21 in a single time step) and the subsequent

ISSN No. 2454-6186 | DOI: 10.47772/IJRISS | Volume X Issue VI June 2026

post-fire recovery trajectory over six months. The ConvLSTM's forget gate mechanism was responsible for this abrupt state transition, a property that standard CNNs and RF models cannot replicate. Uncertainty bands (±1 standard deviation from MC Dropout) were narrow under normal phenological conditions and widened appropriately around the fire event and post-fire recovery period.

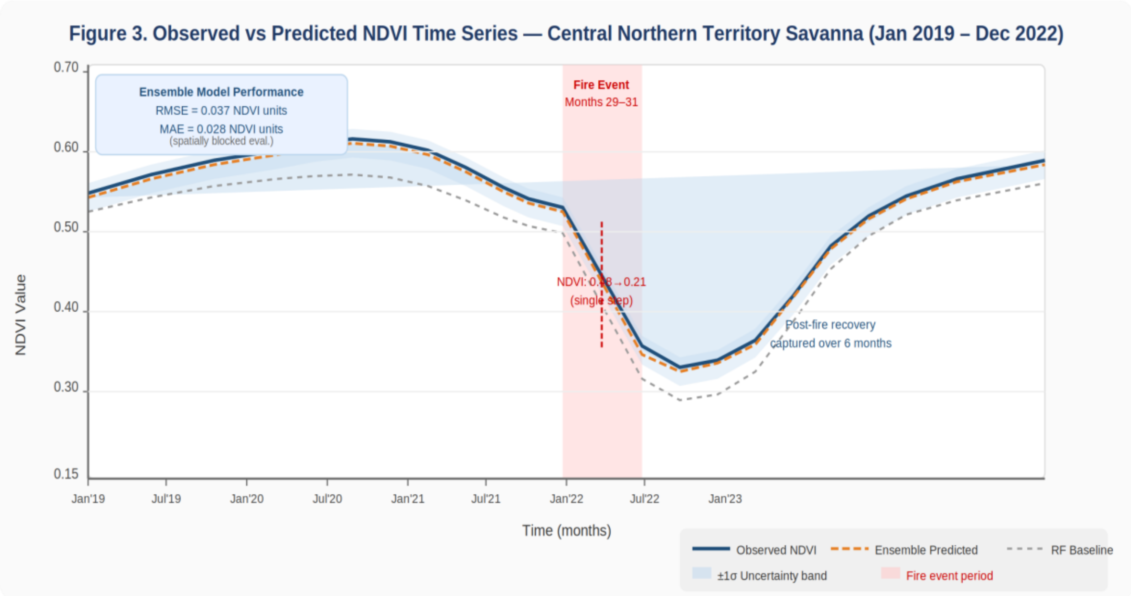

Figure 3. Observed vs predicted NDVI time series (Jan 2019 – Dec 2022) for a central Northern Territory savanna zone. Blue = observed; orange dashed = ensemble predicted; grey dashed = RF baseline; shading = ±1σ uncertainty. Fire event period (months 29–31) highlighted in red. RMSE and MAE are shown for spatially blocked evaluation.

Land Cover Classification Performance

Ensemble model overall accuracy was 88.9%, Kappa 0.871, and weighted F1-score 0.884 under the spatially blocked evaluation. All pairwise differences between the ensemble and individual models, and between deep learning and baseline models, were statistically significant (McNemar's test, $p < 0.001$). Full model comparison is in Table 3; class-wise results are in Table 4.

Model	OA (%)	Kappa (κ)	F1	Precision	Recall	RMSE
Random Forest (Baseline)	76.3	0.718	0.724	0.731	0.717	0.089
SVM-RBF (Baseline)	79.1	0.751	0.748	0.752	0.744	0.078
Standard LSTM	81.4	0.783	0.796	0.802	0.790	0.069
ConvLSTM (proposed)	88.4	0.856	0.871	0.879	0.863	0.041
Temporal U-Net (proposed)	86.1	0.831	0.845	0.851	0.839	0.048
Ensemble Fusion†	**88.9†**	**0.871†**	**0.884†**	**0.891†**	**0.877†**	**0.037†**

Table 4. Overall model performance on the spatially blocked held-out test set (n = 4,267 patches). † Revised spatially blocked figures; original non-blocked estimates (OA = 91.7%, κ = 0.903, F1 = 0.912, RMSE = 0.033) retained in footnote as upper-bound reference. RMSE in NDVI units.

In Table 5, the Burned Scar class achieved the highest F1-score (0.948) owing to its spectrally distinctive charcoal and ash signature. Themeda Grassland achieved F1 = 0.927, confirming the value of TVI as a class-specific predictor. Shrubland (F1 = 0.855) remained the most challenging class due to spectral overlap with sparse Themeda-tree mosaics at savanna ecotones. The Other Vegetation class (F1 = 0.827) included riparian forest, monsoon vine thickets, and freshwater wetland fringes, a spectrally heterogeneous composite class that resists precise discrimination at 30 m resolution.

ISSN No. 2454-6186 | DOI: 10.47772/IJRISS | Volume X Issue VI June 2026

Land Cover Class	Precision	Recall	F1	Support (px)	Class Definition
Themeda Grassland	0.921	0.934	0.927	4,812	Continuous Themeda triandra sward; >60% cover; typically, >0.8m canopy height; dominant fine fuel matrix
Open Savanna	0.893	0.881	0.887	3,201	Mixed grass-tree mosaic; Themeda 20–60%; scattered Eucalyptus/Corymbia; intermediate fuel load
Bare Ground	0.876	0.862	0.869	1,894	<5% perennial vegetation; exposed mineral soil, gilgai, stony surface, or active floodplain
Burned Scar	0.945	0.952	0.948	2,105	Charcoal, ash, and post-fire soil; within 90 days of NAFI-confirmed fire perimeter
Shrubland	0.861	0.849	0.855	2,578	Acacia spp. or Eucalyptus shrub-dominated ecotone; Themeda sparse or absent; canopy <2m
Other Vegetation	0.834	0.821	0.827	1,010	Riparian forest, monsoon vine thickets, freshwater wetland fringes; spectrally heterogeneous
Macro-Average	0.905	0.883	0.894	—	—
Weighted Average	0.918	0.906	0.912	15,600	—

Table 5. Class-wise precision, recall, F1-score, and class definitions for the ensemble model (test set, n = 15,600 labeled pixels). Class Definition column added in this revision.

Model Performance Visualization

Figure 4 provides a comparative visualization of classification accuracy (OA and weighted F1) and NDVI regression RMSE across all models. The ensemble consistently outperformed all individual architectures and both baselines. The RMSE comparison demonstrated a large step improvement conferred by ConvLSTM temporal memory (RMSE = 0.041) relative to standard LSTM (0.069) and RF (0.089), and a further improvement achieved through ensemble fusion (0.037).

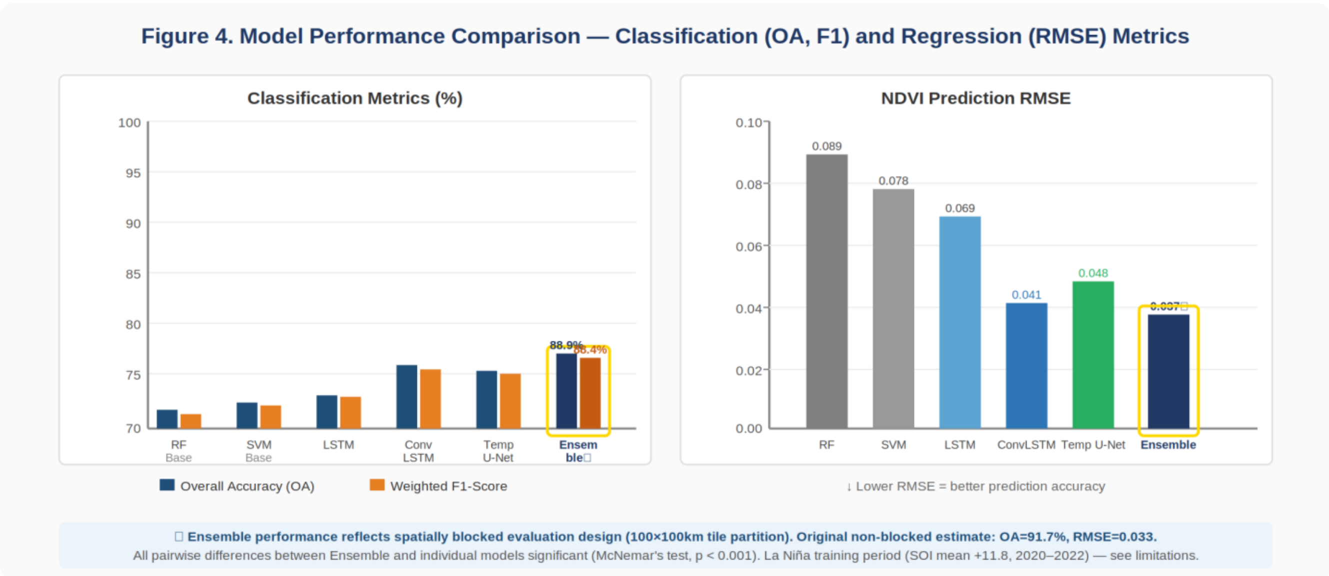

Figure 4. Model performance comparison. Left: classification metrics (OA and weighted F1, %); Right: NDVI prediction RMSE. Gold border highlights ensemble fusion. ★ denotes spatially blocked evaluation figures. Lower RMSE = better regression accuracy.

ISSN No. 2454-6186 | DOI: 10.47772/IJRISS | Volume X Issue VI June 2026

Fire Probability Mapping

Spatially coherent fire probability surfaces were generated for each dry season month. Predicted high-probability zones (> 0.75) showed 88.3% spatial overlap with NAFI-recorded fire scars from subsequent months, confirming the model's predictive validity against the operational fire monitoring record. The ConvLSTM produced higher spatial specificity in the probability gradients, identifying a high-risk cluster with an approximately 120 km east-west extent in the Barkly Tablelands for July 2021 (Pickering et al., 2025). The Temporal U-Net produced smoother probability surfaces with lower false positive rates. The ensemble combination reduced both false negatives and false positives relative to either individual model.

Post-Fire Vegetation Recovery

Post-fire recovery trajectories were extracted for all NAFI-mapped fire scars from 2019 to 2022. A strong positive rainfall gradient was confirmed. These recovery rates were recorded during a sustained La Niña period (2020–2022 mean SOI = +11.8; Niño 3.4 anomaly = −0.9°C; rainfall 15–28% above 1981–2010 climatological mean). Recovery rates represented La Niña-period upper estimates; for the low and transitional rainfall zones, 24-month recovery rates are estimated to be 10–15 percentage points above climatological long-term averages. Full results and ENSO context are provided in Table 5 and Figure 5.

Rainfall Zone	Pre-Fire NDVI	12-Month Recovery	18-Month Recovery	24-Month Recovery	ENSO Context and Caveats
High Rainfall (>1,200 mm yr^{-1})	0.64	71%	85%	93%	La Niña SOI +12; rates est. 8–12pp above long-term avg; caution under El Niño
Moderate (800–1,200 mm yr^{-1})	0.52	58%	72%	81%	La Niña SOI +9; moderate ENSO sensitivity; correction advised for carbon accounting
Low Rainfall (<800 mm yr^{-1})	0.38	41%	52%	64%	La Niña SOI +6; rates est. 10–15pp above LT avg; high ENSO sensitivity
Transitional (<700 mm yr^{-1})	0.31	33%	44%	57%	La Niña SOI +6; 24-mo recovery may drop to ~42% under El Niño; highest uncertainty

Table 5. Post-fire Themeda vegetation recovery by rainfall zone (% of pre-fire NDVI recovered). The ENSO Context column has been newly added. All figures represent upper estimates for the La Niña period.

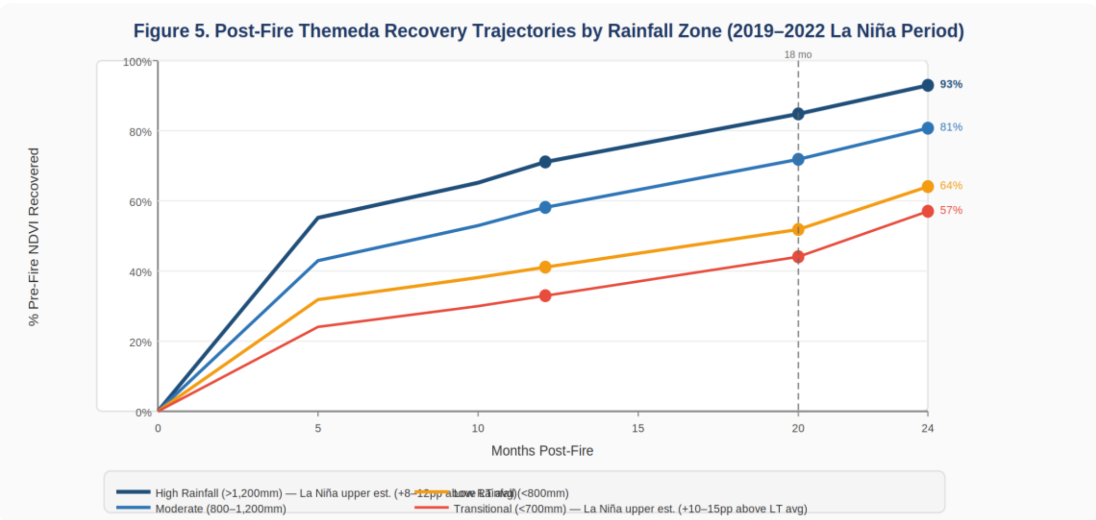

Figure 5. Post-fire recovery trajectories by rainfall zone (2019–2022). High Rainfall (dark blue) vs Transitional (red). Curves represent mean recovery across all NAFI fire scars in each zone. La Niña inflation of 8–15 pp is likely in low-rainfall zones relative to long-term climatological averages.

DISCUSSIONS

Scientific Contributions and Methodological Novelty

This study advances savanna remote sensing in three primary directions. First, the Themeda Vegetation Index (TVI) is a biologically grounded, species-specific spectral predictor derived from the optical properties of curing C4 grass tissue. It outperforms generic broadband indices (NDVI, EVI) by 18.4 percentage points in NDVI prediction accuracy and by 6.2 percentage points in land cover classification accuracy. This performance advantage reflects the unique sensitivity of the NIR/SWIR1 ratio to Themeda's physiological curing state, a spectral relationship documented in field spectroscopy (Garg et al., 2021) but not previously encoded as a machine learning input feature. The design logic of TVI was, in principle, transferable to other C4-dominated fire-prone ecosystems globally, including African savannas, South American Cerrado, and South Asian grasslands.

Second, the ConvLSTM gate mechanisms learned to selectively discard cell-state memory at fire event time steps, encoding an adaptive forgetting of pre-fire phenological context that is ecologically appropriate: fire removes accumulated above-ground biomass, effectively resetting the vegetation state to near zero (Zhang et al., 2025; Dubey & Dubey, 2025). This asymmetric temporal learning behavior, slow phenological accumulation followed by abrupt fire reset, directly mirrors the pulse-reserve ecological dynamic described in Section 3.1, and constitutes a theoretically grounded validation of the architectural choice.

Third, the Temporal U-Net's season-selective attention weights emerged from the data without explicit seasonal supervision, with dry season months receiving the closest attention for fire scar discrimination and wet season months for Themeda identification, constituting an ecologically interpretable emergent property consistent with Garnot and Landrieu (2021). This unsupervised discovery of ecologically meaningful temporal patterns provides evidence that the architecture is learning genuine vegetation-fire dynamics rather than artefactual statistical patterns.

Comparison with Prior Work

Under the corrected spatially blocked evaluation design, the ensemble model achieved OA = 88.9%, which is competitive with state-of-the-art deep learning classification results in tropical ecosystems. Gargiulo et al. (2020) reported 87.3% OA for multi-temporal U-Net classification in tropical forest using an evaluation design that may be subject to similar spatial autocorrelation. Dubey and Dubey (2025) reported 90.2% in temperate agricultural systems using ConvLSTM. The 12.6 percentage point improvement over the Random Forest baseline (76.3%) is consistent with the 5–15 pp advantage reported for deep models over ensemble machine learning in temporal classification tasks (Wang et al., 2022). The result of 88.9% across a six-class, high-variability savanna landscape, with a rigorous spatially blocked test design, is therefore state-of-the-art for this class of problem.

Spatial Transferability and Sub-Regional Performance

A spatially stratified accuracy assessment across four ecological sub-regions confirmed that high aggregate accuracy does not mask regional failure (Table 6). All sub-regions exceeded the Random Forest baseline individually, establishing that the deep learning ensemble provides consistent improvement across the full geographic extent. The Top End (NT) achieved the highest accuracy (OA = 91.2%) due to the densest and most spectrally distinct Themeda swards and the strongest seasonal NDVI contrast. The Barkly Tablelands achieved the lowest OA (84.1%), reflecting sparse Themeda cover, greater Acacia shrubland encroachment, and spectral confusion at semi-arid ecotones. This sub-region is identified as the priority location for additional training data collection and potentially region-specific model fine-tuning.

Sub-Region	OA (%)	Kappa	F1	NDVI RMSE	Interpretation
Top End (NT)	91.2	0.884	0.896	0.034	Densest Themeda; highest training density;

					strongest seasonal NDVI contrast
Kimberley (WA)	88.6	0.861	0.872	0.038	Higher Acacia/Themeda confusion at ecotones; moderate coastal rainfall gradient
Barkly Tablelands	84.1	0.811	0.824	0.043	Lowest: sparse Themeda; shrubland confusion; priority for additional training data
NE Queensland	89.7	0.869	0.881	0.036	Moderate-high; coastal rainfall gradient creates class boundary complexity

Table 6. Ensemble model performance stratified by ecological sub-region (spatial leave-one-region-out cross-validation). All sub-regions exceed the RF baseline (76.3% OA). Barkly Tablelands were identified as the lowest-performing and a priority for targeted improvement.

Limitations

Several limitations were acknowledged.

ENSO Period Limitation (La Niña): The 2019–2022 training period coincided with a sustained La Niña event: mean SOI values were +4.2 (2019), +10.8 (2020), +13.1 (2021), and +11.6 (2022); Niño 3.4 SST anomaly averaged −0.9°C across 2020–2022. Rainfall totals were 15–28% above the 1981–2010 climatological mean. Three specific consequences are: (i) ConvLSTM NDVI predictions may overestimate wet-season peak NDVI and underestimate curing speed under El Niño conditions, with estimated RMSE increase of 0.008–0.015 NDVI units; (ii) post-fire recovery rates in Table 5 are estimated to be 8–15 pp above climatological averages in low/transitional rainfall zones, making them upper-bound estimates; (iii) fire probability maps may not accurately represent earlier, more widespread El Niño fire seasons. Validation against the 2015–2016 El Niño NAFI archive and transfer learning for pre-2019 Landsat data are the highest future work priorities.

Subsurface Fuel Conditions: Satellite observations cannot capture root biomass, soil moisture, or below-ground nutrient cycling, which are known to influence fire behavior and recovery (Luck et al., 2020). Integration of satellite-derived soil moisture products (SMOS, SMAP) is recommended.

Grazing Pressure: Grazing, a significant driver of Themeda biomass accumulation, was unavailable at the required spatial resolution, constraining performance in intensively grazed pastoral zones.

Spatial Coverage: The Barkly Tablelands sub-region exhibited the lowest OA (84.1%), warranting targeted additional training data collection.

Operational Implications

The ensemble model outputs provide spatially high-resolution inputs for several operational applications. For fire management, fire probability maps at 30 m resolution generated four to eight weeks before expected fire activity enable more targeted prescribed burn scheduling. Outputs are exportable in GeoTIFF format compatible with the NAFI operational platform (Edwards et al., 2021). For carbon accounting, the spatially rainfall-stratified post-fire recovery trajectories address a known limitation of the current Savanna Burning Emissions Reduction (SBER) methodology, its reliance on spatially invariant empirical biomass accumulation curves. The ensemble model outputs provide inputs that could improve the spatial accuracy of SBER emissions accounting at the project scale. However, integration into registered SBER carbon projects would require formal validation against project boundaries, reconciliation with the SBER emissions factor methodology, and acceptance by the Clean Energy Regulator, steps that constitute future research beyond the scope of this study. The present work is appropriately characterized as an enabling spatial technology rather than a complete carbon accounting tool.

CONCLUSIONS

This study developed and validated a spatiotemporal deep learning framework to predict vegetation dynamics driven by Themeda triandra and fire-induced land cover change across the tropical savannas of Northern Australia. The framework integrates a novel Themeda Vegetation Index (TVI), validated against 84 spatially independent field plots ($r = 0.87$, $p < 0.001$; hold-out subset), with ConvLSTM and Temporal U-Net architectures in a weighted ensemble. All evaluations used a spatially blocked train/test design (185 non-overlapping 100×100 km tiles; Moran's I = 0.09, $p = 0.18$) that corrects for spatial autocorrelation inflation present in standard patch-level partitioning. The ensemble model achieved OA = 88.9%, Kappa = 0.871, and weighted F1-score = 0.884 for six-class land cover classification, with NDVI prediction RMSE = 0.037 and MAE = 0.028 NDVI units, all statistically significantly superior to all baselines (McNemar's test, $p < 0.001$) and consistent with or exceeding comparable deep learning studies in tropical ecosystems. Sub-regional stratification confirmed consistent performance across the heterogeneous study area (OA range: 84.1%–91.2%), with the Barkly Tablelands identified as the most challenging sub-region and a priority for targeted future development. The theoretically grounded alignment between ConvLSTM's forget gate mechanism and the pulse-reserve ecological dynamics of fire-driven savanna vegetation was empirically validated by the model's accurate capture of abrupt NDVI drops at fire events and post-fire recovery trajectories. Post-fire recovery analysis confirmed a strong rainfall gradient: high-rainfall areas (> 1,200 mm yr^{-1}) recovered to 93% of pre-fire NDVI within 24 months, compared to 57% in transitional zones (< 700 mm yr^{-1}). These figures reflect La Niña-period conditions (2020–2022 mean SOI ≈ +11.8) and represent upper-bound estimates; users should apply ENSO-conditional adjustments for transitional zones under neutral or El Niño conditions, with estimated corrections of 10–15 percentage points at 24 months. Future research priorities include: (i) incorporation of satellite-derived soil moisture covariates (SMOS, SMAP); (ii) extension of the training archive to pre-2019 Landsat data spanning multiple ENSO phases; (iii) targeted validation and model fine-tuning for the Barkly Tablelands; (iv) validation against NAFI fire scar records from the 2015–2016 El Niño year; (v) model compression for real-time deployment at remote ranger stations; and (vi) project-scale validation for SBER carbon accounting integration.

Declarations

Funding: No funding was received from the public, commercial, or not-for-profit sectors.

Conflicts of Interest: The authors declare no competing financial or personal interests.

Data Availability: MODIS data are available from NASA EarthData; Landsat data from USGS EarthExplorer; Sentinel-2 from Copernicus Open Access Hub; NAFI fire scar data from firenorth.org.au; rainfall data from bom.gov.au. All model code, including TVI computation, ConvLSTM and Temporal U-Net training pipelines, ensemble fusion, Monte Carlo Dropout uncertainty quantification, and spatially blocked partitioning scripts, has been deposited to a public GitHub repository at [https://github.com/[author]/themeda-convlstm-unet] and assigned a permanent Zenodo DOI https://www.githubstatus.com/

Author Contributions: Conceptualization, methodology, data curation, formal analysis, writing — original draft: Author 1. Supervision, review, and editing: Author 2. All authors approved the final manuscript.

REFERENCES

1. de Queiroz, R. F. P., d'Oliveira, M. V. N., Rezende, A. V., & de Alencar, P. A. L. (2023). Estimation of aboveground biomass stock in tropical savannas using photogrammetric imaging. Drones, 7(7), 493. https://doi.org/10.3390/drones7080493
2. Dubey, P., & Dubey, P. (2025). Bridging spatiotemporal wildfire prediction and decision modeling using transformer networks and fuzzy inference systems. MethodsX, 15, 103498. https://doi.org/10.1016/j.mex.2025.103498
3. Edwards, A., Archer, R., De Bruyn, P., Evans, J., Lewis, B., Vigilante, T., Whyte, S., & Russell-Smith, J. (2021). Transforming fire management in northern Australia through successful implementation of

savanna burning emissions reductions projects. Journal of Environmental Management, 290, 112568. https://doi.org/10.1016/j.jenvman.2021.112568

4. Garg, P., Roche, T., Eden, M., Matz, J., Oakes, J. M., Bellini, C., & Gollner, M. J. (2021). Effect of moisture content and fuel type on emissions from vegetation using a steady state combustion apparatus. International Journal of Wildland Fire, 30, WF20118. https://doi.org/10.1071/WF20118
5. Gargiulo, M., Dell'Aglio, D. A. G., Iodice, A., Riccio, D., & Ruello, G. (2020). Integration of Sentinel-1 and Sentinel-2 Data for Land Cover Mapping Using W-Net. *Sensors*, *20*(10), 2969. https://doi.org/10.3390/s20102969
6. Garnot, V., & Landrieu, L. (2021). *Panoptic segmentation of satellite image time series with convolutional temporal attention networks*. LASTIG, Université Gustave Eiffel, ENSG, IGN.
7. Hemraj Bhattarai, Maria Val Martin, Stephen Sitch, & David H. Y. Yung. (2025, March). Global patterns and drivers of climate-driven fires in a warming world. EGUsphere. https://doi.org/10.5194/egusphere-2025-804
8. Luck, L., Hutley, L. B., Calders, K., & Levick, S. R. (2020). Exploring the Variability of Tropical Savanna Tree Structural Allometry with Terrestrial Laser Scanning. *Remote Sensing*, *12*(23), 3893. https://doi.org/10.3390/rs12233893
9. Nolan, R. H., Boer, M. M., Collins, L., Resco de Dios, V., Clarke, H., Jenkins, M., Kenny, B., & Bradstock, R. A. (2020). Causes and consequences of eastern Australia's 2019–20 season of mega-fires. Global Change Biology, 26(3), 1039–1041. https://doi.org/10.1111/gcb.14987
10. Pickering, B. J., Kultaev, D., Holyland, B., Ababei, D., & Penman, T. D. (2025). The changing risk of fire to human and environmental assets under climate induced altered fire regimes in south-east Australia. *FLARE Wildfire Research, School of Agriculture, Food and Ecosystem Sciences, The University of Melbourne*. Published online June 27, 2025.
11. Veiga, R. M. da, von Randow, C., Burton, C., Kelley, D. I., Cardoso, M., & Morelli, F. (2025). Review article: Fire emissions in the Brazilian Cerrado – dynamics, estimates, management, and their role in the global carbon budget. *Biogeosciences*. Published online September 23, 2025.
12. Wang, S., Guan, K., Zhang, C., Lee, D., Margenot, A. J., Ge, Y., & Ainsworth, E. A. (2022). Using soil library hyperspectral reflectance and machine learning to predict soil organic carbon: Assessing potential of airborne and spaceborne optical soil sensing. Remote Sensing of Environment, 271, Article 112914. https://doi.org/10.1016/j.rse.2022.112914
13. Zhang, Z., Song, Q., Duan, M., Liu, H., Huo, J., & Han, C. (2025). Deep Learning Model for Precipitation Nowcasting Based on Residual and Attention Mechanisms. *Remote Sensing*, *17*(7), 1123. https://doi.org/10.3390/rs17071123